Mon. Not. R. Astron. Soc. **000**, 1–**??** (2011) Printed 12 December 2013 (MN LaTeX style file v2.2)

arXiv:1301.0060v2 [astro-ph.CO] 29 May 2013

On the accuracy of the Perturbative Approach for Strong Lensing: Local Distortion for Pseudo-Elliptical Models

Habib S. Dúmet-Montoya[1,2⋆], Gabriel B. Caminha[1,2], Bruno Moraes[1,2], Martin Makler[1,2],
Mandeep S. S. Gill[3,4], and Basílio X. Santiago[2,5]
[1] *Instituto de Cosmologia, Relatividade e Astrofísica — ICRA, Centro Brasileiro de Pesquisas Físicas*
Rua Dr. Xavier Sigaud 150, CEP 22290-180, Rio de Janeiro, RJ, Brazil
[2] *Laboratório Interinstitucional de e-Astronomia — LIneA,*
Rua Gal. José Cristino 77, CEP 20921-400, Rio de Janeiro, RJ, Brazil
[3] *Kavli Institute for Particle Astrophysics & Cosmology, SLAC National Accelerator Laboratory*
2575 Sand Hill Road, Menlo Park, CA 94025, USA
[4] *Center for Cosmology and Astro-Particle Physics, Department of Physics, The Ohio State University*
191 West Woodruff Avenue, Columbus, OH 43210
[5] *Departamento de Astronomia, Universidade Federal do Rio Grande do Sul*
Av. Bento Gonçalves 9500, Porto Alegre, RS 91501-970, Brazil

12 December 2013

ABSTRACT

The Perturbative Approach (PA) introduced by Alard (2007) provides analytic solutions for gravitational arcs by solving the lens equation linearized around the Einstein ring solution. This is a powerful method for lens inversion and simulations in that it can be used, in principle, for generic lens models. In this paper we aim to quantify the domain of validity of this method for three quantities derived from the linearized mapping: caustics, critical curves, and the deformation cross section (i.e. the arc cross section in the infinitesimal circular source approximation). We consider lens models with elliptical potentials, in particular the Singular Isothermal Elliptic Potential and Pseudo-Elliptical Navarro–Frenk–White models. We show that the PA is exact for this first model. For the second, we obtain constraints on the model parameter space (given by the potential ellipticity parameter ε and characteristic convergence κ_s) such that the PA is accurate for the aforementioned quantities. In this process we obtain analytic expressions for several lensing functions, which are valid for the PA in general. The determination of this domain of validity could have significant implications for the use of the PA, but it still needs to be probed with extended sources.

Key words: galaxies:cluster:general, cosmology: dark matter, gravitational lensing: strong.

1 INTRODUCTION

Gravitational arc systems can be used as a powerful probe of the matter distribution of galaxies and galaxy clusters acting as lenses (Kovner 1989; Miralda-Escudé 1993a; Hattori et al. 1997). Further, their abundance can be used to constrain cosmological models (Bartelmann et al. 1998; Oguri et al 2001; Golse et al. 2002; Bartelmann et al. 2003). This motivated several arc searches to be carried out, both in wide field surveys (Gladders et al. 2003; Estrada et al. 2007; Cabanac et al. 2007; Belokurov et al. 2009; Kubo et al. 2010; Kneib et al. 2010; Gilbank et al. 2011; Wen et al. 2011; More et al. 2012; Bayliss 2012; Wiesner et al. 2012, Erben et al. 2012, in prep.), as well as in images targeting know clusters (Luppino et al. 1999; Zaritsky & Gonzalez 2003; Smith et al. 2005; Sand et al. 2005; Hennawi et al. 2008; Kausch et al. 2010; Horesh et al. 2010; Furlanetto et al. 2012). Upcoming wide field imaging surveys, such as the Dark Energy Survey[1] (DES; Annis et al. 2005; Abbott et al. 2005), which started operations in 2012, are expected to detect of the order of 10^3 strong lensing systems, about an order of magnitude increase with respect to the current largest surveys.

Two primary approaches have been followed in practical applications of gravitational arc systems. On the one hand, *inverse modelling* attempts to "deproject" the arcs in individual lens systems to determine lens and source properties (Kneib et al. 1993; Keeton 2001a; Golse et al. 2002; Comerford et al. 2006; Wayth & Webster 2006; Jullo et al. 2007, 2010). On the other hand, *arc statistics* (Wu & Hammer 1993; Grossman & Saha 1994;

⋆ E-mail: hdumetm@cbpf.br

[1] `www.http://www.darkenergysurvey.org/`

Bartelmann & Weiss 1994) aims at counting the number of arcs in cluster samples and comparing with the predictions from cosmological models.

Both approaches require the lens equation to be solved numerically for finite sources numerous times. The inverse modelling typically needs arc images obtained from a multidimensional space of source positions and lens parameters scanned during the minimization process to find the best solution for sources and lenses (e.g., Wayth & Webster 2006). For this reason analyses using the inverse modelling are often restricted to simple lens models, in particular models with elliptic lens potentials (so-called pseudo-elliptical) and/or to point sources, for example, considering bright spots in arcs as multiple images of point sources (Keeton 2001a; Wayth & Webster 2006; Jullo et al. 2007; Oguri 2010).

For arc statistics, predictions for the arc cross section must be derived as a function of source and lens properties and the cosmological model, again by obtaining a large set of arc images (Miralda-Escudé 1993b; Bartelmann & Weiss 1994; Meneghetti et al. 2001, 2003; Oguri et al. 2003). The cross section is then convolved with the distribution of lens properties expected in a given cosmology and convolved with the source distribution. Another approach is to use directly high resolution N-body simulations obtaining arc images by ray-tracing through the mass distribution for a large number of sources (Horesh et al. 2011; Meneghetti et al. 2008; Boldrin et al. 2012).

It is therefore useful to develop approximate methods for obtaining gravitational arcs, which will be particularly useful given the increase of strong lensing systems to be discovered by the next generation wide-field surveys. A most promising technique for this purpose is given by the Perturbative Approach (Alard 2007, 2008), which provides an approximate solution for the lens equation close to the Einstein ring, leading to analytic solutions for arcs.

The power of this approach is that it can be applied, in principle, to generic lens models, including those arising from simulations. The method is suitable for large tangential arcs, since the solutions are accurate for images located close to the Einstein ring corresponding to the circularly averaged lensing potential.

Another important feature of the method is that it naturally reproduces arcs resulting from the merger of multiple images, which cannot be accounted for with other approximate methods for arcs proposed in the literature (e.g., Keeton 2001b; Fedeli et al. 2006). Such merger arcs are key for lens inversion methods and also play an important role in the arc cross section (Rozo et al. 2008).

The Perturbative Approach has already been used for inverse modelling in Alard (2009, 2010). Given that it reproduces arc contours that can be associated to isophotes, it could also be used to simulate the brightness distribution of arcs, in a similar way to what was implemented in Furlanetto et al. (2013) for arc shaped contours.

An important issue for practical applications of this approach is the determination of its domain of validity. This topic is discussed in Alard (2007), comparisons with arc simulations are presented in Peirani et al. (2008), and a recent work by Habara & Yamamoto (2011) has investigated arcs in several configurations for a pseudo-elliptical model in this approach. However a systematic study of its limit of applicability has not yet been carried out. In this paper we make a first attempt to determine a domain of validity of the method in terms of the parameter space of the lens model. We will restrict to the simple case of pseudo-elliptical models, which are nevertheless widely used for the inverse modelling. Moreover, for simplicity, we will restrict the comparisons with the exact solution for three quantities connected to arcs, but which do not involve the lensing of finite sources. We expect that the limits here obtained can be connected to the domain of validity for arcs and extended for more general models, but this is left to subsequent explorations.

In this work, our purpose is twofold. The first is to explore the application of the Perturbative Approach to determine quantities arising from the local lens mapping, such as the arc cross section for infinitesimal circular sources (deformation cross section). The second is to determine a domain of validity such that the critical curves, caustics, and deformation cross section are accurately obtained. This study is performed for the pseudo-elliptical Navarro–Frenk–White model (PNFW), determining regions of its parameter space where the Perturbative Approach provides a good approximation for these quantities. We also consider the Singular Isothermal Elliptic Potential (SIEP) model and show that the solution of the Perturbative Approach is exact in this case.

The outline of this paper is as follows: in Sec. 2 we present a few basic results of gravitational lensing theory, introduce the radial lens models to be used in this work, and discuss models with elliptic lensing potentials. In Sec. 3 we review the Perturbative Approach, present its application to the computation of the deformation cross section, and discuss its implementation to pseudo-elliptical models. In Sec. 4 we establish a metric for the comparison between the Perturbative Approach and the exact solution for critical curves and caustics and determine a domain of validity for the Perturbative approach. In Sec. 5 we summarize the results and present concluding remarks.

2 BASICS OF GRAVITATIONAL LENSING: DEFINITIONS AND NOTATION

In this section we present a brief review of the lensing theory to set up the notation and to define the quantities associated with pseudo-elliptical models. For a more detailed description see, e.g., chap. 8 of Schneider et al. (1992), chap. 6 of Petters et al. (2001) and chap. 3 of Mollerach & Roulet (2002).

The *lens equation* relates the two-dimensional position (with respect to the optical axis) of the observed images $\boldsymbol{\xi}$ to those of the sources $\boldsymbol{\eta}$. We may choose a a length scale ξ_0 and define $\boldsymbol{x} = \boldsymbol{\xi}/\xi_0$ and $\boldsymbol{y} = \boldsymbol{\eta}/\eta_0$, with $\eta_0 \equiv \frac{D_{\rm OS}}{D_{\rm OL}}\xi_0$, where $D_{\rm OL}, D_{\rm OS}$ are the angular diameter distances from the observer to the lens and source respectively. Using these definitions the lens equation is written as

$$\boldsymbol{y} = \boldsymbol{x} - \boldsymbol{\alpha}(\boldsymbol{x}) = \boldsymbol{x} - \nabla_{\boldsymbol{x}}\varphi(\boldsymbol{x}), \tag{1}$$

where $\boldsymbol{\alpha}(\boldsymbol{x})$ is the "dimensionless" deflection angle and $\varphi(\boldsymbol{x})$ is the "dimensionless" *lensing potential*,

The local distortion in the lens plane is described by the Jacobian matrix of eq. (1)

$$\mathbf{J} = \left(\frac{\partial \boldsymbol{y}}{\partial \boldsymbol{x}}\right)_{ij} = \delta_{ij} - \partial_i \alpha_j(\boldsymbol{x}). \tag{2}$$

The two eigenvalues of this matrix are written as $\lambda_r = 1 - \kappa + \gamma$ and $\lambda_t = 1 - \kappa - \gamma$, where κ and γ are the convergence and the shear given below. Points satisfying the conditions $\lambda_{r,t} = 0$ define the radial and tangential critical curves respectively. Mapping these curves onto the source plane, we obtain the caustics.

For axially symmetric models the deflection angle, convergence and shear are given by

$$\alpha(x) = \frac{d\varphi_0(x)}{dx} = x\frac{\bar{\Sigma}(\xi_0 x)}{\Sigma_{\rm crit}}, \tag{3}$$

$$\kappa(x) = \frac{1}{2}\left[\frac{\alpha(x)}{x} + \frac{d\alpha(x)}{dx}\right], \tag{4}$$

$$\gamma(x) \quad = \quad \frac{1}{2}\left[\frac{\alpha(x)}{x} - \frac{d\alpha(x)}{dx}\right]. \tag{5}$$

where $\bar{\Sigma}(\xi_0 x)$ is the mean surface density within a radius x and $\Sigma_{\rm crit}$ is the critical surface density.

In this work, one model we will make use of is the Singular Isothermal Sphere (SIS), which is useful to model lenses at the galactic scale. Its dimensionless lensing potential, deflection angle, convergence and shear are given by (Turner et al. 1984; Schneider et al. 1992; van de Ven et al. 2009)

$$\varphi_0(x) = x, \;\; \alpha(x) = 1, \;\; \kappa(x) = \gamma(x) = \frac{1}{2}, \tag{6}$$

where we choose the Einstein Radius to be the characteristic scale

$$\xi_0 = R_{\rm E} = \frac{\sigma_v^2}{G\Sigma_{\rm crit}},$$

where σ_v is the velocity dispersion. From this potential analytic solutions of the lens equation can be obtained for finite sources (Dobler & Keeton 2006; Dúmet-Montoya 2011).

We will also make use of the Navarro–Frenk–White model (Navarro et al. 1996, 1997, hereafter NFW), often used to represent lenses in the galaxy to galaxy cluster mass scales. This model has two independent parameters r_s and ρ_s. By fixing $\xi_0 = r_s$ and defining the characteristic convergence as

$$\kappa_s = \frac{\rho_s r_s}{\Sigma_{\rm crit}}, \tag{7}$$

the lensing potential is given by (Bartelmann 1996)

$$\varphi_0(x) = 4\kappa_s \left(\frac{1}{2}\log^2\frac{x}{2} - 2\,{\rm arctanh}^2\sqrt{\frac{1-x}{1+x}}\right), \tag{8}$$

which is a function of the parameter κ_s alone.

Models with elliptical potentials (the so-called pseudo-elliptical models) provide simple analytical solutions for some lensing quantities (Blandford & Kochanek 1987; Kassiola & Kovner 1993; Kneib 2001). They have been widely used in lens inversion problems and are implemented in several public codes for lens inversion such as *Gravlens* (Keeton 2001a), *Lensview* (Wayth & Webster 2006), *Lenstool* (Jullo et al. 2007), and *glafic* (Oguri 2010). They have also been used for arc simulations (Oguri 2002; Meneghetti et al. 2003, 2007).

Pseudo-elliptical models, with potential $\varphi_\varepsilon(\boldsymbol{x})$, are built from a given axially symmetric potential $\varphi_0(x)$ by replacing the radial coordinate x by

$$\tilde{x} = \sqrt{a_1\, x_1^2 + a_2\, x_2^2} = x\Delta_\phi, \tag{9}$$

where

$$\Delta_\phi \equiv \sqrt{a_1\, \cos^2\phi + a_2\, \sin^2\phi}, \tag{10}$$

such that the ellipticity of the lensing potential is

$$\varepsilon_\varphi = 1 - \sqrt{\frac{a_1}{a_2}},$$

where the orientation was chosen such that the major axis of the ellipse is along the x_1 axis (i.e., $a_2 > a_1$). The deflection angle, convergence, and shear can be written as combinations of the lensing functions of the corresponding axially symmetric model for any choice of a_1 and a_2 (Dúmet-Montoya et al. 2012).

The SIEP and PNFW models are obtained by following this procedure for the potentials given in eqs. (6) and (8), respectively.

3 PERTURBATIVE APPROACH

For a given lens model, the Perturbative Approach allows one to obtain analytic solutions for arcs as perturbations of the Einstein Ring solution. In this work we investigate the limits of applicability of the Perturbative Approach, by considering simple non-axially symmetric models and by looking at local properties of the lens mapping, instead of lensed finite sources.

In this section we briefly review the Perturbative Approach and use it for the derivation of the caustics and critical curves, the deformation cross section and quantities needed for its computation. The method is also applied to models with elliptical lensing potentials.

3.1 Lens Equation

The gist of the Perturbative Approach for gravitational arcs developed by Alard (2007, 2008) is to obtain an analytic solution for the lens equation considering the lens as a perturbation of an axially symmetric configuration and the source position as a small deviation from the optical axis (i.e., positioned transversely away from perfect observer–lens–source alignment). In other words, the arcs are found as perturbations of the Einstein Ring configuration. In this work we will consider the thin lens and the single lens plane approximations, which imply a unique solution for the Einstein Ring (Werner et al. 2008).

The Einstein Ring is the image of a source aligned with an axially symmetric lens (with lensing potential φ_0). Its radius $x_{\rm E}$ is obtained by solving the $\lambda_t(\boldsymbol{x}) = 0$ at the centre of the source plane, i.e.

$$x - \frac{d\varphi_0}{dx} = 0. \tag{11}$$

Arcs can be obtained by perturbing the equation above either by shifting the position of the source away from the optical axis and/or by adding a non-circular perturbation to the lensing potential. These perturbations are described by

$$\boldsymbol{y} = \delta y, \;\; \varphi(\boldsymbol{x}) = \varphi_0(x) + \delta\psi(\boldsymbol{x}). \tag{12}$$

These perturbations are assumed to be of the same order in ϵ (the strength of the perturbation) throughout the following calculations, such that

$$\delta y = \epsilon\overline{y}, \;\; \delta\psi(\boldsymbol{x}) = \epsilon\overline{\varphi}(\boldsymbol{x}).$$

The response to such perturbations is given by the displacement of the radial coordinate in the lens plane[2], i.e., $x = x_{\rm E} \to x = x_{\rm E} + \delta x$ where we also assume the same order in ϵ such that $\delta x = \epsilon\overline{x}$.

To find $\epsilon\overline{x}$ we solve eq. (1) by expanding the solution around $x = x_{\rm E}$. Expanding the lensing potential in a Taylor series around $x = x_{\rm E}$, we have

$$\varphi(\boldsymbol{x}) = \sum_{n=0}^{\infty}\left[C_n + f_n(\phi)\right](\epsilon\overline{x})^n, \tag{13}$$

where

$$C_n \quad \equiv \quad \frac{1}{n!}\left[\frac{d^n\varphi_0}{d\,x^n}\right]_{x=x_{\rm E}},$$

---

[2] Note that in Alard (2007, 2008) $\xi_0 = x_{\rm E}$ was used as a characteristic scale. This choice is equivalent to setting $x_{\rm E} = 1$ in our equations. In this work we have made the choice of keeping $x_{\rm E}$ explicitly in the equations for more generality, allowing us, for example, to choose another characteristic scale of the problem.

$$f_n(\phi) \equiv \frac{1}{n!}\left[\frac{\partial^n \delta\psi}{\partial x^n}\right]_{x=x_{\rm E}} = \frac{\epsilon}{n!}\left[\frac{\partial^n \overline{\varphi}}{\partial x^n}\right]_{x=x_{\rm E}}. \tag{14}$$

Inserting $x = x_{\rm E} + \epsilon\overline{x}$ and (13) into eq. (1), we find that the resulting equation at zeroth order in ϵ is

$$x_{\rm E} = C_1, \tag{15}$$

which is the Einstein Ring equation. Using the relations above and $\delta x = \epsilon\overline{x}$, the resulting equation at the first order in ϵ is given by

$$\begin{aligned} y_1 &= (\kappa_2\delta x - f_1)\cos\phi + \frac{1}{x_{\rm E}}\frac{df_0}{d\phi}\sin\phi, \\ y_2 &= (\kappa_2\delta x - f_1)\sin\phi - \frac{1}{x_{\rm E}}\frac{df_0}{d\phi}\cos\phi, \end{aligned} \tag{16}$$

where $\kappa_2 \equiv 1 - 2C_2$. From eqs. (3)–(5) we have

$$\frac{d^2\varphi_0(x)}{dx^2} = 2\kappa(x) - \frac{\alpha(x)}{x},$$

and therefore κ_2 can be expressed as

$$\kappa_2 = 2 - 2\kappa(x_{\rm E}). \tag{17}$$

Eq. (16) is the lens equation in the Perturbative Approach. It can be solved for δx for each angular position ϕ of the source, given a perturbation described by $f_n(\phi)$. To obtain the images of a finite source, we must first parametrize its boundary. Then, by varying ϕ from 0 to 2π, each point of that boundary is mapped to the lens plane through eqs. (16). As a result, a new equation with separated radial and angular components is formed, whose solution is obtained straightforwardly (Alard 2007, 2008; Peirani et al. 2008; Dúmet-Montoya 2011)

It is important emphasize that the solutions (x_i, ϕ_i) of eq. (16) are valid only to first order in the perturbations in eq. (12), i.e. only for points near the Einstein Ring. For points far from this curve, the solutions are not expected to be highly accurate. For this reason, the Perturbative Approach is particularly useful for applications involving tangential arcs. In this work, instead of using finite sources, we focus on the potential applicability of this method to quantities based on the local mapping as a first step to quantify the differences with the exact solutions.

3.2 Local Mapping

The Jacobian matrix for the lens mapping is

$$\mathbf{J} = \left(\frac{\partial \boldsymbol{y}}{\partial \boldsymbol{x}}\right)_{ij} = \sum_k \left(\mathbf{J}_{S\to L,pol}\right)_{ik}\left(\mathbf{J}_{L,pol\to cart}\right)_{kj}, \tag{18}$$

where $\mathbf{J}_{S\to L,pol}$ is the Jacobian of the transformation from the lens plane to the source plane in polar coordinates from eq. (16) and $\mathbf{J}_{L,pol\to cart}$ is the standard Jacobian matrix from polar to Cartesian coordinates. The calculation of the eigenvalues of the lens mapping is then straightforward from the equation above and they are given by

$$\begin{aligned} \lambda_t &= -\tfrac{1}{x}\left[\tfrac{1}{x_{\rm E}}\tfrac{d^2 f_0}{d\phi^2} - (\kappa_2\delta x - f_1)\right], \\ \lambda_r &= \kappa_2. \end{aligned} \tag{19}$$

Therefore, the radial coordinate of the tangential critical curve is

$$x_t(\phi) = x_{\rm E} + \delta x_t(\phi) = x_{\rm E} + \frac{1}{\kappa_2}\left(f_1 + \frac{1}{x_{\rm E}}\frac{d^2 f_0}{d\phi^2}\right), \tag{20}$$

and the parametric equations of the critical curve are simply

$$\begin{aligned} x_{1t} &= x_t(\phi)\cos\phi, \\ x_{2t} &= x_t(\phi)\sin\phi. \end{aligned}$$

Inserting δx_t in eq. (16), the parametric equations of the tangential caustic are found to be

$$\begin{aligned} y_{1t} &= \frac{1}{x_{\rm E}}\frac{d^2 f_0}{d\phi^2}\cos\phi + \frac{1}{x_{\rm E}}\frac{df_0}{d\phi}\sin\phi, \\ y_{2t} &= \frac{1}{x_{\rm E}}\frac{d^2 f_0}{d\phi^2}\sin\phi - \frac{1}{x_{\rm E}}\frac{df_0}{d\phi}\cos\phi. \end{aligned} \tag{21}$$

3.3 Constant Distortion Curves

For infinitesimal circular sources, the length-to-width ratio of arcs can be approximated by the ratio of the eigenvalues of the lens mapping Jacobian matrix (Wu & Hammer 1993; Bartelmann & Weiss 1994; Hamana & Futamase 1997)

$$\frac{L}{W} \simeq |R_\lambda(\boldsymbol{x})| \equiv \left|\frac{\lambda_r(\boldsymbol{x})}{\lambda_t(\boldsymbol{x})}\right|. \tag{22}$$

Under this approximation, it is possible to define a region where gravitational arcs are expected to form by fixing a value for the threshold length to width ratio $R_{\rm th}$. Such region is limited by the curves $R_\lambda = \pm R_{\rm th}$ (constant distortion curves). Although the condition (22) does not hold for merger arcs (Rozo et al. 2008), nor for large or elliptical sources, the curves defined above still provide a typical scale for the region of arc formation. In this work, we adopt the common choice $R_{\rm th} = 10$ (unless explicitly stated otherwise). We denote the radial coordinates of these curves as x_λ. They are obtained by solving $R_\lambda(\boldsymbol{x}) = \pm R_{\rm th}$, with λ_r and λ_t given in the Perturbative Approach by eq. (19). It follows that

$$x_\lambda(\phi) = x_t(\phi) \times \begin{cases} \frac{R_{\rm th}}{R_{\rm th}-1}, & R_\lambda = +R_{\rm th}, \\[2ex] \frac{R_{\rm th}}{R_{\rm th}+1}, & R_\lambda = -R_{\rm th}. \end{cases} \tag{23}$$

The constant distortion curves in the lens plane are therefore self-similar to the tangential critical curve. The mapping of these curves to the source plane is done by substituting $\delta x_\lambda = x_\lambda - x_{\rm E}$ in eq. (16). For instance, the curve $R_\lambda = +R_{\rm th}$ has the following parametric equations

$$\begin{aligned} y_{1\lambda} &= \tfrac{f_1+\kappa_2 x_{\rm E}}{R_{\rm th}-1}\cos\phi + \tfrac{1}{x_{\rm E}}\left[\left(\tfrac{R_{\rm th}}{R_{\rm th}-1}\right)\tfrac{d^2 f_0}{d\phi}\cos\phi + \tfrac{df_0}{d\phi}\sin\phi\right], \\ y_{2\lambda} &= \tfrac{f_1+\kappa_2 x_{\rm E}}{R_{\rm th}-1}\sin\phi + \tfrac{1}{x_{\rm E}}\left[\left(\tfrac{R_{\rm th}}{R_{\rm th}-1}\right)\tfrac{d^2 f_0}{d\phi}\sin\phi - \tfrac{df_0}{d\phi}\cos\phi\right]. \end{aligned} \tag{24}$$

The parametric equations of the $R_\lambda = -R_{\rm th}$ curve are given by the expressions above with the substitution $R_{\rm th} - 1 \rightarrow R_{\rm th} + 1$. There is no self-similarity between these curves and the tangential caustics.

3.4 Deformation Cross Section

As mentioned in the introduction, the *arc cross section* is a key ingredient in arc statistics calculations. Is is defined as the effective area in the source plane such that sources within it will be mapped into images with $L/W \geqslant R_{\rm th}$. The definition of this area must take into account the image multiplicity given the source position (i.e. multiply-imaged regions are counted multiple times, see e.g., Meneghetti et al. 2003). The computation of the arc cross section in general demands ray-tracing simulations, which are computationally expensive (Miralda-Escudé 1993b; Bartelmann & Weiss 1994;

Meneghetti et al. 2001, 2003; Oguri et al. 2003). An alternative is to use the infinitesimal circular source approximation, eq. (22), which allows the computation of the arc cross section to be carried out directly from the local mapping from lens to source plane. In this case, $\sigma_{R_{\rm th}}$ is computed in the lens plane by

$$\sigma_{R_{\rm th}} = \eta_0^2 \tilde{\sigma}_{R_{\rm th}} = \eta_0^2 \int_{|R_\lambda| \geqslant R_{\rm th}} \frac{d^2\, x}{|\mu(\boldsymbol{x})|} \tag{25}$$

(see, e.g., Fedeli et al. 2006; Dúmet-Montoya et al. 2012; Caminha et al. 2013), where $\mu = (\lambda_r \lambda_t)^{-1}$ is the magnification and the integral is performed over the region of arc formation above the chosen threshold. The quantity $\tilde{\sigma}_{R_{\rm th}}$ is known as the dimensionless deformation cross section.

In the Perturbative Approach, the magnification can be written from eq. (19) as

$$|\mu(\boldsymbol{x})|^{-1} = \frac{\kappa_2^2}{x} \begin{cases} x_t(\phi) - x, & x < x_t(\phi), \\ \\ x - x_t(\phi), & x > x_t(\phi), \end{cases} \tag{26}$$

where $x_t(\phi)$ is given in eq. (20). Inserting the equation above in eq. (25) and integrating the radial coordinate within the lower and upper limits given in eq. (23), it is straightforward to obtain

$$\tilde{\sigma}_{R_{\rm th}} = \kappa_2^2 \frac{|R_{\rm th}|^2 + 1}{(|R_{\rm th}|^2 - 1)^2} \int_0^{2\pi} x_t^2(\phi)\, {\rm d}\phi. \tag{27}$$

Note that $\tilde{\sigma}_{R_{\rm th}} \propto R_{\rm th}^{-2}$ for $R_{\rm th} \gg 1$, as expected from the behaviour of the deformation cross section with $R_{\rm th}$ (Rozo et al. 2008; Caminha et al. 2013).

For axially symmetric models ($x_t = x_{\rm E}$) the cross section is given simply by

$$\tilde{\sigma}_{R_{\rm th}} = 2\pi \kappa_2^2 x_{\rm E}^2 \frac{R_{\rm th}^2 + 1}{(R_{\rm th}^2 - 1)^2}. \tag{28}$$

The expression above is exact for the SIS model (Bartelmann et al. 1995). For other axially symmetric models this expression is still an approximation, since the curves $R_\lambda = \pm R_{\rm th}$ are obtained approximatively.

3.5 Perturbative Functions for Pseudo-Elliptical Models

We write the elliptical potential as

$$\varphi_\varepsilon(\boldsymbol{x}) = \varphi_0(x) + \left[\varphi_0(\tilde{x}) - \varphi_0(x)\right], \tag{29}$$

such that the perturbed potential becomes

$$\delta\psi(x,\phi) = \varphi_0(\tilde{x}) - \varphi_0(x).$$

From the definitions (14) and using the identities (3)–(5), it follows that

$$\begin{aligned} f_1 &= \frac{\tilde{x}_{\rm E}}{x_{\rm E}} \alpha(\tilde{x}_{\rm E}) - \alpha(x_{\rm E}), \\ \frac{df_0}{d\phi} &= \frac{x_{\rm E}^2}{2\tilde{x}_{\rm E}} \alpha(\tilde{x}_{\rm E})(a_2 - a_1)\sin 2\phi, \\ \frac{d^2 f_0}{d\phi^2} &= \frac{x_{\rm E}^2}{\tilde{x}_{\rm E}} \alpha(\tilde{x}_{\rm E})(a_2 - a_1)\cos 2\phi \\ &\quad - \frac{\gamma(\tilde{x}_{\rm E})}{2} \left[\frac{x_{\rm E}^2}{\tilde{x}_{\rm E}}(a_2 - a_1)\sin 2\phi\right]^2, \end{aligned} \tag{30}$$

where α and γ are the deflection angle and shear of the corresponding axially symmetric lens. These expressions hold for any parametrization of the lensing potential ellipticity and for any pseudo-elliptical lens (Dúmet-Montoya et al. 2012).

For small values of the lensing potential ellipticity, eqs. (30) reduce to

$$\begin{aligned} f_1 &= \frac{a_1 - a_2}{2} \kappa(x_{\rm E}) x_{\rm E} \cos 2\phi \, + \mathcal{O}(\epsilon^2), \\ \frac{df_0}{d\phi} &= \frac{a_2 - a_1}{2} x_{\rm E}^2 \sin 2\phi \, + \mathcal{O}(\epsilon^2), \\ \frac{d^2 f_0}{d\phi^2} &= (a_2 - a_1) x_{\rm E}^2 \cos 2\phi \, + \mathcal{O}(\epsilon^2). \end{aligned} \tag{31}$$

From eq. (20) and the expressions above, we have

$$x_t(\phi) = x_{\rm E} \left[1 + \frac{a_2 - a_1}{2} \left(\frac{2 - \kappa(x_{\rm E})}{\kappa_2}\right) \cos 2\phi\right], \tag{32}$$

and inserting this into eq (27) we get

$$\tilde{\sigma}_{R_{\rm th}} = 2\pi x_{\rm E}^2 \frac{R_{\rm th}^2 + 1}{(R_{\rm th}^2 - 1)^2} \left[\kappa_2^2 + \frac{1}{8}\left(1 + \frac{\kappa_2}{2}\right)^2 (a_2 - a_1)^2\right]. \tag{33}$$

Thus, for small ellipticities, the deviation with respect to the axially symmetric case is quadratic.

Instead of using a_2 and a_1 it is more intuitive to express the results in terms of the ellipticity of the potential. Several parameterizations have been used to define the ellipticity in this context. From now on, we adopt the convention (Blandford & Kochanek 1987; Golse & Kneib 2002; Dúmet-Montoya et al. 2012)

$$a_1 = 1 - \varepsilon, \quad a_2 = 1 + \varepsilon, \tag{34}$$

where ε is the potential ellipticity parameter. The connection to the ellipticity of the mass distribution ε_Σ depends on the model. For the SIEP $\varepsilon_\Sigma = 3\,\varepsilon$ to first order in ε (Kassiola & Kovner 1993). For the PNFW model this relation depends on κ_s and expressions for $\varepsilon_\Sigma(\varepsilon, \kappa_s)$ are provided in Dúmet-Montoya et al. (2012).

Fig. 1 shows the comparison for caustics and critical curves between the Perturbative Approach and the exact solution for the PNFW model for different values of κ_s and ε.

3.6 Singular Isothermal Elliptic Potential

One of the simplest and most often used lens models is given by the SIEP. For this model, using expressions (6) in Eq. (30), the perturbative functions are

$$\begin{aligned} f_1 &= \Delta_\phi - 1, \\ \frac{df_0}{d\phi} &= (a_2 - a_1) \frac{\sin 2\phi}{2\Delta_\phi}, \\ \frac{d^2 f_0}{d\phi^2} &= a_1\, a_2 \Delta_\phi^{-3} - \Delta_\phi, \end{aligned} \tag{35}$$

where Δ_ϕ is given in eq. (10). When substituted into eqs. (16) the expressions above lead to

$$y_1 = x\left(1 - \frac{a_1}{\tilde{x}}\right)\cos\phi \;\text{ and }\; y_2 = x\left(1 - \frac{a_2}{\tilde{x}}\right)\sin\phi, \tag{36}$$

which are the components of the lens equation of this model without any approximation. Hence, the solution of the Perturbative Approach is exact in the case of lensing by the SIEP model.

The same conclusion does not hold for the PNFW model. We will thus investigate the domain of validity for this model in the next section.

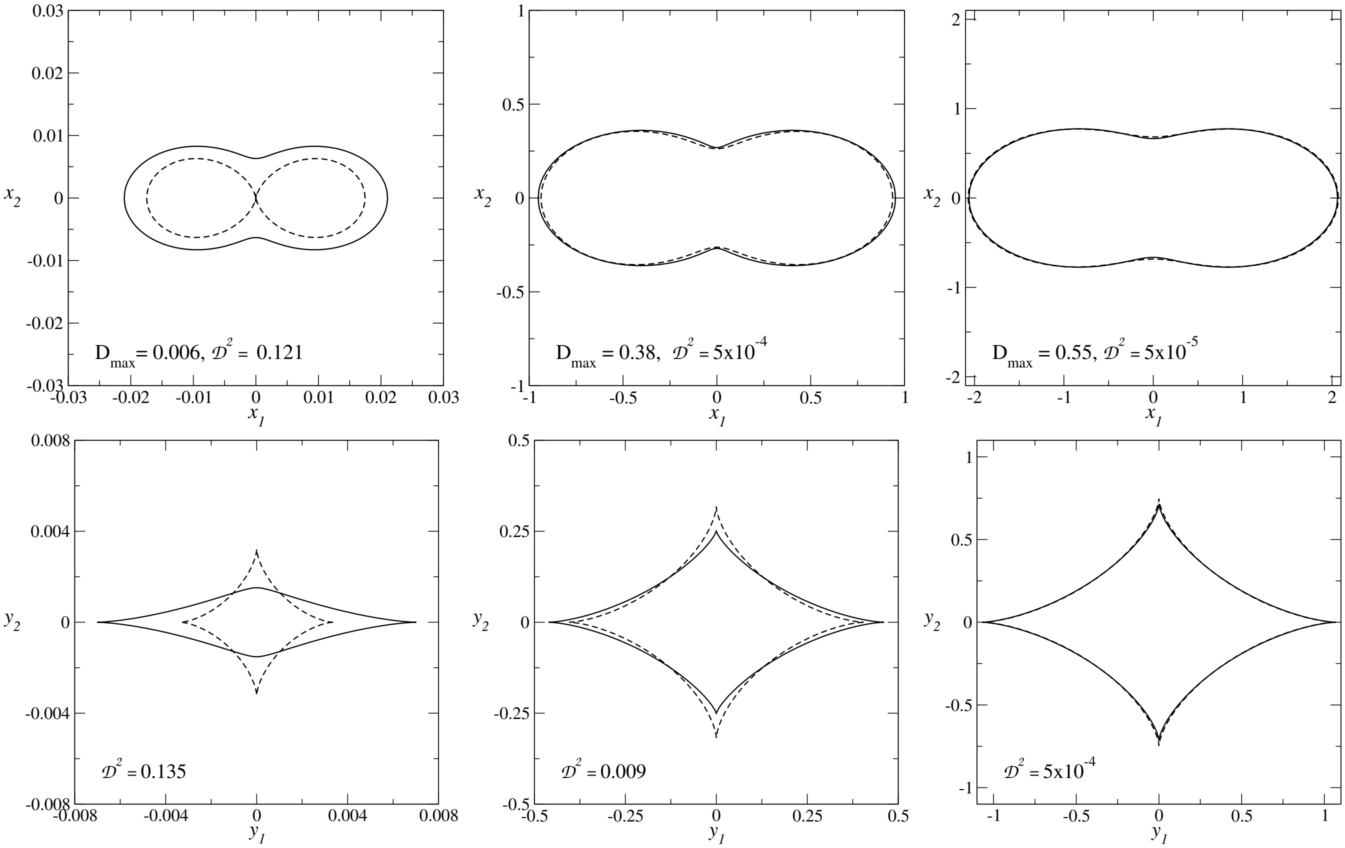

Figure 1. Critical curves (top panels) and caustics (bottom panels) obtained with the Perturbative Approach (dashed lines) and the exact solution (solid lines) for the PNFW model: $\kappa_s = 0.1$ and $\varepsilon = 0.2$ (left), $\kappa_s = 0.5$ and $\varepsilon = 0.32$ (middle) and $\kappa_s = 1.0$ and $\varepsilon = 0.35$ (right). The values of ε in the middle and right panels were chosen by imposing $\mathcal{D}^2 = 5 \times 10^{-4}$ for critical curves and caustics, respectively (see Sec. 4).

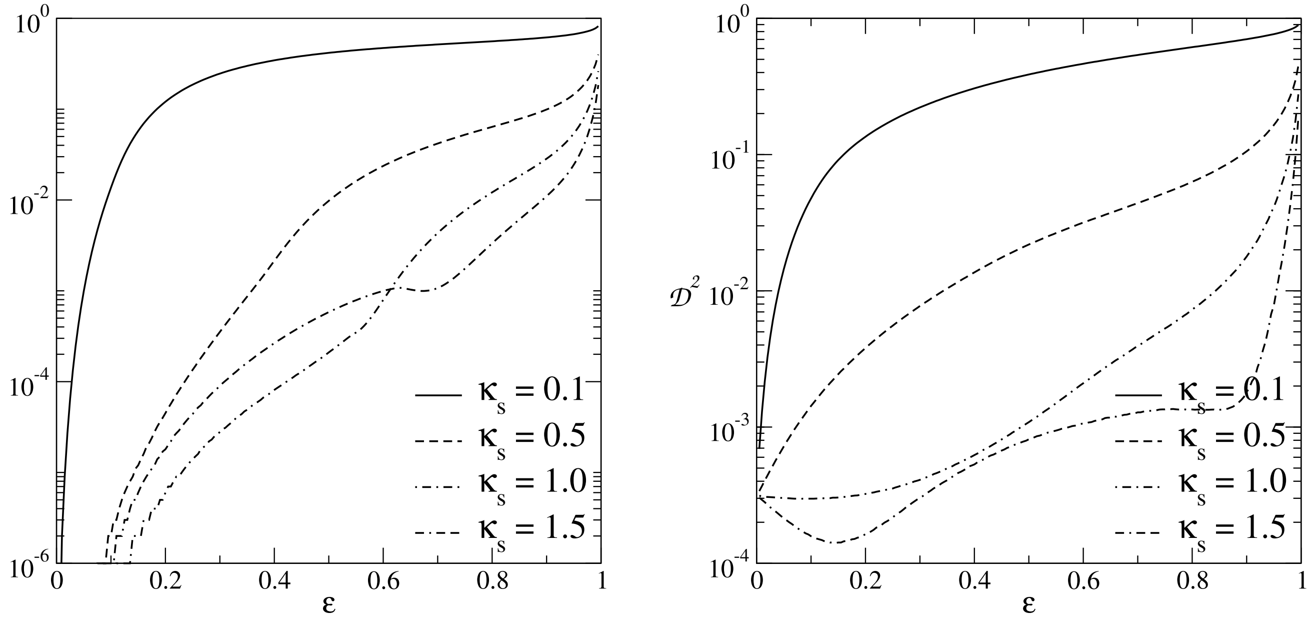

Figure 2. Mean weighted squared radial fractional difference $\mathcal{D}^2$ as a function of the ellipticity parameter for the PNFW model for various values of the characteristic convergence κ_s. Left Panel: For Critical Curves. Right Panel: For Caustics.

4 LIMITS OF VALIDITY OF THE PERTURBATIVE APPROACH FOR THE PNFW MODEL

Previous attempts to quantify the differences between exact and perturbative solutions were carried out in the literature. Alard (2007) proposed a method based on the relative importance of the third-order term in the Taylor series of the gravitational potential. Habara & Yamamoto (2011) performed a qualitative analysis of a particular arc configuration, varying some of the system parameters and establishing criteria based on the position and multiplicity of the images. However, they did not define a metric to compare the solutions nor carry on the analysis for more general configurations.

Investigating the domain of validity of the Perturbative Approach with finite sources would require a large parameter space to be probed, including the lens and source parameters and their relative positions. On the other hand, as a starting point, we may look at quantities that are dependent only on the lens, such as the tangential caustic and critical curve and the deformation cross section (the latter will depend also on the choice of $R_{\rm th}$). Besides reducing the parameter space — for example, for ε and κ_s in the PNFW case — it is simpler to define metrics to quantify the deviation of the perturbed solution from the exact one. We expect that the constraints on the domain of validity determined from the quantities above can be connected to those arising from the images of finite sources. Thus, exploring the simplest case before may provide guidance to the determination of the domain of validity of the method finite sources in the future. Setting a domain of validity from the lens model alone may provide a rapid method to adjudicate validity of the Perturbative Method *a priori*, just from the lensing potential, without the need of obtaining images of the sources.

In this section, we shall attempt to quantify the deviation of critical curves and caustics using a figure-of-merit akin to the one proposed in Dúmet-Montoya et al. (2012). We will then compare the deformation cross sections and, finally, combine the results to obtain limits that define a region in the parameter space of PNFW models where the Perturbative Approach can be used to accurately obtain local properties of a given lens system.

4.1 Limits for critical curves and caustics

To quantify the deviation of the solution of the Perturbative Approach from the exact one for critical curves and caustics we use a figure-of-merit defined as the mean weighted squared fractional radial difference between the curves, i.e.[3]

$$\mathcal{D}^2 \equiv \frac{\sum_{i=1}^{N} w_i [x_{\rm ES}(\phi_i) - x_{\rm PA}(\phi_i)]^2}{\sum_{i=1}^{N} w_i \, x_{\rm ES}^2(\phi_i)}, \qquad (37)$$

where $x_{\rm ES}(\phi_i)$ and $x_{\rm PA}(\phi_i)$ are the radial coordinates of the tangential curves (either critical curves or caustics) obtained from the exact solution and with the Perturbative Approach, respectively. These are computed on a discrete set of N points defined by the polar angle ϕ_i. Further, $w_i \equiv \phi_i - \phi_{i-1}$ is a weight to account for a possible non-uniform distribution of points in ϕ.

Choosing a cut-off value for $\mathcal{D}^2$, we can define a range in ε for which the curves obtained with both the exact and perturbative solutions will be similar enough to each other. The cut-off value is then chosen by visually comparing the exact and perturbative solutions for the critical curves and caustics associated with several values of $\mathcal{D}^2$, for combinations of the PNFW lens parameters.

Before presenting the results, we should stress a technical point. In the particular case of caustics, calculating the two functions in the same polar angle becomes a non-trivial issue. This is because in general, the source plane points (y_{1t}, y_{2t}) are not equally distributed in angle, as they are obtained scanning angular values in the lens plane which map nonlinearly to angular values in the source plane. Thus in general, a source plane angle does not correspond to the same lens plane angle. Yet, to compute $\mathcal{D}^2$ for the caustics, it is necessary that both $x_{\rm ES}$ and $x_{\rm PA}$ be calculated at the same polar angle position in the source plane. Thus, to enforce this last point, we first determine the polar angle corresponding to each point (y_{1t}, y_{2t}) obtained with the exact solution, i.e.,

$$\phi_S = \arctan\left(\frac{y_{2t}}{y_{1t}}\right)$$

and obtain the corresponding radial coordinate $x_{\rm ES} = y_t(\phi_S) = \sqrt{y_{1t}^2 + y_{2t}^2}$. In the same way, we compute the polar angle of the tangential caustic obtained with the Perturbative Approach (which we denote by $\phi_S^{\rm PA}$), i.e.,

$$\phi_S^{\rm PA} = \arctan\left(\frac{y_{2t}(\phi_L)}{y_{1t}(\phi_L)}\right),$$

where y_{1t} and y_{2t} are given in eq. (21) and $y_t^{\rm PA} = \sqrt{y_{1t}^2 + y_{2t}^2}$. We then vary the angle ϕ_L (only the interval $0 \leqslant \phi_L \leqslant \pi/2$ is needed, for symmetry reasons) such that for each radial position y_t, the angles ϕ_S and $\phi_S^{\rm PA}$ are chosen to have the same value at step i. Finally, having determined (y_t, ϕ_S) for the exact solution and $(y_t^{\rm PA}, \phi_S^{\rm PA})$ we proceed to compute $\mathcal{D}^2$ as in eq. (37).

Fig. 2 shows $\mathcal{D}^2$ as a function of ε for some values of[4] κ_s. In the left panel, the results for critical curves are shown. Since the perturbation increases with ε, $\mathcal{D}^2$ also increases with ε, as we might expect. In addition, $\mathcal{D}^2$ decreases as κ_s increases, at least for $\kappa_s < 1.0$. In the right panel, we show the results for caustics. The behaviour of $\mathcal{D}^2$ is qualitatively similar to that of critical curves, except for at the highest κ_s, where the behaviours are reversed. However, the values of $\mathcal{D}^2$ computed for caustics are higher than the corresponding ones for critical curves, for a given (κ_s, ε). This means that imposing cut-off values of $\mathcal{D}^2$ for matching caustics, we will match the corresponding critical curves automatically. We found by visual inspection that for $\mathcal{D}^2 \leqslant 5 \times 10^{-4}$ there is a very good match for the caustic curves. In Fig. 1 we show the values of $\mathcal{D}^2$ calculated for each example, demonstrating visually the validity of this diagnostic measure. In particular, we have checked that cut-off values of $\mathcal{D}^2$ higher but close to our chosen limit of 5×10^{-4} are not suited for matching caustic curves well.

To estimate the validity of the Perturbative Approach, Alard (2007) introduced the parameter $D \equiv 3|C_3|(\delta x_{\rm arc})^2$, where $\delta x_{\rm arc}$ corresponds to the difference between the *arc contours* obtained in the perturbative approach and the Einstein radius, and C_3 is the third-order term in the Taylor expansion of the gravitational potential (see eq. 13). In order for the Perturbative Approach to be accurate, D should be small. For models based on the SIS profile, this condition is always true, since $C_3 = 0$ (which is consistent with the fact that the Perturbative Method is exact in this case). For other pseudo-elliptical models, usually $C_3 \neq 0$.

---

[3] Expression (37) is formally equal to the one proposed in Dúmet-Montoya et al. (2012), where it was used to compare an iso-contour of κ to an ellipse. Here the same expression is used to compare two solutions for caustics or critical curves.

[4] Throughout this work, following Dúmet-Montoya et al. (2012), we will consider the range $\kappa_s \leqslant 1.5$.

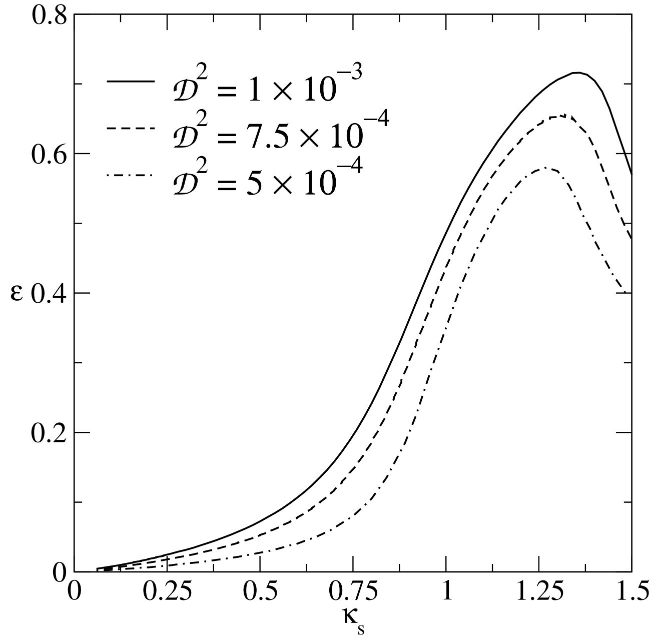

Figure 3. Maximum values of ε obtained from some cut-off values of $\mathcal{D}^2$ on caustics for the PNFW model.

Here we adapt the definition of D to be used for critical curves, such that δx is now the radial deviation of these curves with respect to x_E. We associate a unique value of D to the tangential critical curve, using its maximum value over this curve, which corresponds to

$$D_{\max} = 3|C_3|\max\{(x_t(\phi) - x_{\rm E})^2\}, \tag{38}$$

where x_t is given in eq. (20) and $0 \leqslant \phi \leqslant 2\pi$. Following Alard's criterion (i.e. $D_{\max} \ll 1$), it would be expected that the critical curves and caustics obtained with the Perturbative Approach would be close to the ones obtained in the exact case when both ε and κ_s are small. We compute $D_{\max}$ for the curves shown in Fig. 1, obtaining $D_{\max} = 0.006$, 0.38 and 0.55 from left to right panels. Contrary to expectations, when $D_{\max}$ increases, the curves obtained with the Perturbative Approach become more similar to the exact solutions. Therefore, the criterion $D_{\max} \ll 1$ does not reflect the validity of the Perturbative Approach for these cases. Moreover, $D_{\max}$ is not scale-invariant (i.e. $D_{\max} \propto r_s^2$, where r_s is the length scale of the PNFW model). These considerations show that this measure is not well-suited to assess the limit of validity of the method for caustics and critical curves. This result emphasizes the relevance of our definition of $\mathcal{D}^2$ as a measure for the validity of the Perturbative Approach for critical curves and caustics.

For the application of our criterion, we define $\varepsilon_{\max}^{\rm PA}$, for a given κ_s, as the ellipticity threshold giving $\mathcal{D}^2 = 5 \times 10^{-4}$. This will be used as a measure of the limit of applicability for the Perturbative Approach for critical curves and caustics. Fig. 3 shows the maximum values of ε as a function of κ_s for the PNFW model, for some cut-off values of $\mathcal{D}^2$. The $\varepsilon_{\max}^{\rm PA}(\kappa_s)$ function shown in this figure is well-fitted by a Padé approximant of the form

$$\varepsilon_{\max}^{\rm PA} = \frac{\sum_{n=0}^{4} a_n(\kappa_s)^n}{\sum_{m=0}^{2} b_m(\kappa_s)^m}, \tag{39}$$

with $a_n = \{-0.018, 0.235, -0.415, 0.565, -0.264\}$ and $b_n = \{2.243, -3.709, 1.725\}$.

4.2 Comparison between Deformation Cross Sections

In this section, we compare the exact and perturbative solutions for the deformation cross section in order to establish limits of validity for the approximation of this quantity. We then contrast these limits to those obtained for caustics and critical curves as done in Sec. 4.1 (i.e. by imposing $\varepsilon < \varepsilon_{\max}^{\rm PA}$ for each κ_s). If within this regime the Perturbative Approach and the exact solution of the deformation cross section do not agree well, this can impose additional limits to the applicability of the Perturbative Approach.

To quantify the difference between the deformation cross sections, we compute their relative difference

$$\frac{\Delta\tilde{\sigma}_{R_{\rm th}}}{\tilde{\sigma}_{R_{\rm th}}} = \left|\frac{\tilde{\sigma}_{\rm ES,R_{th}} - \tilde{\sigma}_{\rm PA,R_{th}}}{\tilde{\sigma}_{\rm ES,R_{th}}}\right|, \tag{40}$$

where the subscripts ES and PA refer to the exact and perturbative calculations, respectively.

In Fig. 4 we show $\Delta\tilde{\sigma}_{10}/\tilde{\sigma}_{10}$ as a function of κ_s for some values of ε. In the left panel we compare the exact solution with the expansion for low ellipticities in the Perturbative Approach, eq. (33), while in the right panel we compare with the general expression, eq. (27) [5]. The perturbative calculation for the axially symmetric NFW model ($\varepsilon = 0$, eq. 28) is a good approximation in this case, since $\Delta\tilde{\sigma}_{10}/\tilde{\sigma}_{10} < 10\%$ for the entire allowed range of κ_s. For values of $\varepsilon < 0.1$ the Perturbative Approach is a good approximation only for $\kappa_s \gtrsim 0.5$. As ε increases, the difference is larger at smaller values of κ_s. However, the perturbative calculation is accurate to within about 10% for $\kappa_s \gtrsim 0.7$ up to $\varepsilon = 0.3$ (see the right panel of Fig. 4).

Additionally, we computed $\Delta\tilde{\sigma}_{\rm th}/\tilde{\sigma}_{\rm th}$ as a function of the threshold $R_{\rm th}$. We find that $\Delta\tilde{\sigma}_{\rm th}/\tilde{\sigma}_{\rm th}$ can exceed 50% at values of $R_{\rm th} \lesssim 2.5$, since for these values of $R_{\rm th}$, the *constant distortion curves* are far from the tangential critical curves, meaning that the premises of the Perturbative Approach do not apply. However, as $R_{\rm th}$ increases, the relative deviations among the deformation cross sections decrease. In particular, we found that for $\kappa_s \gtrsim 0.9$ and $R_{\rm th} > 7.5$, these relative deviations do not depend on $R_{\rm th}$.

In Fig. 5 we show isocontours of $\Delta\tilde{\sigma}_{10}/\tilde{\sigma}_{10}$, for the exact and perturbative calculations, in the parameter space κ_s–ε together with the curve $\varepsilon_{\max}^{\rm PA}(\kappa_s)$. We see that the constraints imposed by $\Delta\tilde{\sigma}_{10}/\tilde{\sigma}_{10}$ and $\varepsilon_{\max}^{\rm PA}$ are complementary, meaning that for $\kappa_s \lesssim 1.0$ the constraint obtained with caustics and critical curves is the strongest, while the opposite is true for $\kappa_s > 1.0$ if we impose that the maximum fractional deviation for the cross section is 10%.

We may then combine the constraints to define a region limited approximately by the curves

$$\varepsilon = \begin{cases} \varepsilon_{\max}^{\rm PA}(\kappa_s), & \kappa_s \lesssim 1.0, \\ 0.33, & \kappa_s > 1.0. \end{cases} \tag{41}$$

Within this region the Perturbative Approach can replace the exact computation of critical curves, caustics, and deformation cross section with high accuracy.

---

[5] It should be noted that, due to the quadratic scaling with respect to ϵ of the deviation from the axially symmetric case, eq. (33) is an excellent approximation for eq. (27) for low ellipticities. Thus the left panel of Fig. 4 would remain essentially unchanged if we used eq. (27) instead of eq. (33) there.

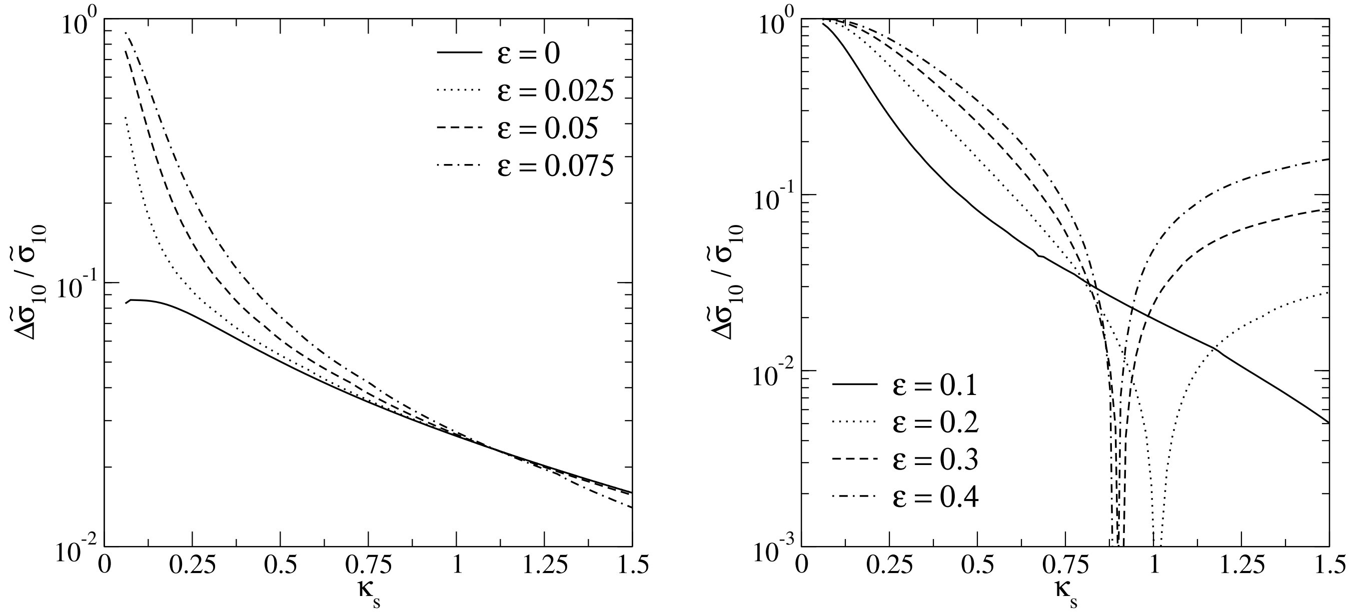

Figure 4. Relative deviation among deformation cross sections for the PNFW model as a function of κ_s for some values of ε. Left panel: $\Delta\tilde{\sigma}_{10}/\tilde{\sigma}_{10}$ between exact solution and eq. (33). Right panel: $\Delta\tilde{\sigma}_{10}/\tilde{\sigma}_{10}$ between exact solution and eq. (27).

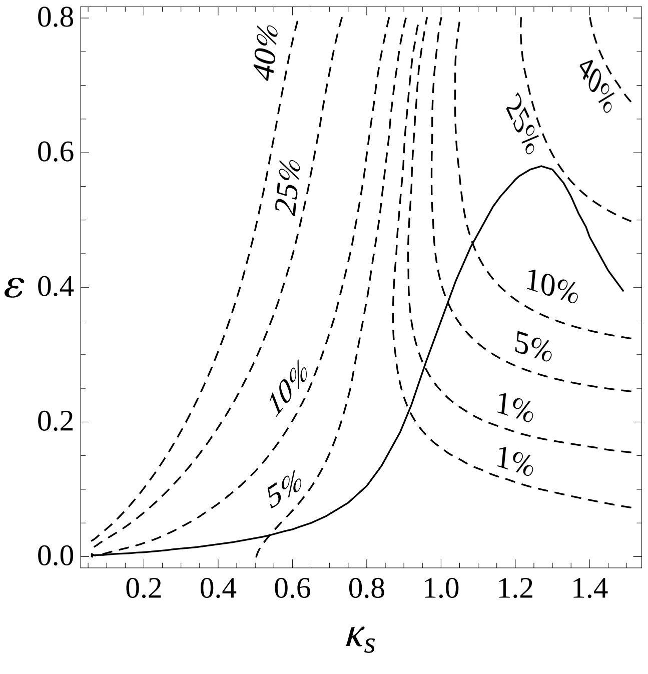

Figure 5. Comparison between deformation cross sections for the PNFW model space parameter. Contours of constant $\Delta\tilde{\sigma}_{10}/\tilde{\sigma}_{10}$. The solid line shows the $\varepsilon^{\rm PA}_{\rm max}(\kappa_s)$ curve.

5 CONCLUDING REMARKS

The Perturbative Approach (Alard 2007, 2008, 2009, 2010) provides analytical solutions for gravitational arcs by solving the lens equation linearised around the Einstein Ring solution. This method has a wide range of potential applications, from the inverse problem in strong lensing to fast arc simulations. This technique goes beyond other analytical approximations in the literature in that it may be used for generic lens models (including mass distributions arising from N-body simulations) and for finite sources.

A key aspect for practical applications of the method that has not been systematically addressed before is the determination of its limit of validity. Motivated by this issue, in this paper we aimed to determine the accuracy of the Perturbative Approach for caustics and critical curves and for the deformation arc cross section. Although these quantities do not involve arcs (i.e. the lensing of finite sources) they allow one to obtain limits on the accuracy of the linearized mapping from the Perturbative Approach. Also, the parameter space to be probed is significantly decreased, since these quantities depend basically on the lens properties and not the source ones.

We have considered a restricted set of lens models, more specifically those with elliptical lens potentials, and in particular the PNFW and SIEP models, which are nevertheless widely used in strong lensing applications, specially for the inverse modelling. Whenever possible, we sought to derive analytic expressions for the quantities involved in the calculations, many of which are new. Some are valid for the Perturbative Approach in general, others apply to pseudo-elliptic lens models. The main results of the paper are summarized below.

We obtained analytic expressions for the constant distortion curves in the Perturbative Approach (eqs. 23 and 24), which, in the lens plane, are found to be self-similar to the tangential critical curve. We derived an analytic formula for the deformation cross section (eq. 27), which reproduces the scaling of the arc cross section with $R_{\rm th}$ obtained numerically in previous works. For axially symmetric models the cross section is obtained in closed form (eq. 28).

We have obtained simple analytic expressions for the perturbative functions for pseudo-elliptical models, which are valid for any choice of the ellipticity parametrization (eq. 30). These expressions generalize those given in Alard (2007, 2008) and in Habara & Yamamoto (2011).

We derive approximate solutions to the tangential critical curve (eq. 32) and for the deformation cross section (eq. 33) for low ellipticities in pseudo-elliptical models. We show that the deviation of the cross section with respect to the axially symmetric case is quadratic in the ellipticity.

We have considered the SIEP and the PNFW models to represent lenses at galaxy and galaxy cluster mass scales. We have shown that the Perturbative Approach provides the exact solution for the SIEP model. For the PNFW model, we compared the critical curves and caustics obtained with this approach with those obtained with the exact solution for a wide range of values of κ_s and ε.

We show that the criterion $D_{\max} \ll 1$ proposed by Alard (2007) extended to be applied the tangential critical curve (eq. 38), is not adequate to set a limit of validity for these cases. To this end, we use a figure-of-merit, $\mathcal{D}^2$ (eq. 37) to quantify the deviation of the Perturbative Approach from the exact solution for caustics and critical curves. We verify that $\mathcal{D}^2$ provides a quantitative description of the deviation among both solutions. In particular, $\mathcal{D}^2$ decreases with κ_s (as can be drawn from Fig. 1) and increases with ε (as expected from the increasing of the perturbation to the lensing potential with ε). Since the deviation between the exact and perturbative solutions for caustics is higher than the deviation for critical curves, it is sufficient to set a limit on $\mathcal{D}^2$ for caustics to ensure a small deviation for critical curves.

By setting a threshold on $\mathcal{D}^2$ computed at caustics, a maximum value of ε is determined for each κ_s, such that a good matching for caustics and also for critical curves is ensured. We determine these maximum values $\varepsilon^{\rm PA}_{\max}(\kappa_s)$ by choosing $\mathcal{D}^2 = 5\times10^{-4}$. This defines a domain of applicability of the Perturbative Approach for the PNFW model in the range of κ_s being considered. We provide a fitting function for $\varepsilon^{\rm PA}_{\max}(\kappa_s)$ (eq. 39). For $\kappa_s \lesssim 0.8$, the Perturbative Approach is limited to $\varepsilon \lesssim 0.1$. However, for $\kappa_s > 1.0$ it is possible to use this approach even up to $\varepsilon = 0.4$ for these cases.

Another limit on the PFNW model parameters is obtained from the comparison of the deformation cross section for both exact and perturbative calculations. The fractional deviation is less than 10% (Fig. 5) for $\kappa_s \gtrsim 0.7$ and $\varepsilon \lesssim 0.3$ (corresponding to $\epsilon_\Sigma \lesssim 0.55$).

We may use these results to set further constraints on the ellipticity parameter of the PNFW model, by requiring an agreement with the exact $\tilde{\sigma}_{R_{\rm th}}$, besides the condition $\varepsilon < \varepsilon^{\rm PA}_{\max}(\kappa_s)$. This ensures that caustics, critical curves, and the local mapping are well reproduced by the Perturbative Approach for the PNFW model. The combined restriction, imposing the matching for caustics and an agreement to about 10% for deformation cross sections, is given in eq. (41).

In this paper we provided a first systematic attempt to set limits on the domain of applicability of the Perturbative Approach for strong lensing in terms of the parameters of a given lens model, more specifically for the PNFW model. The limits are imposed so that the caustics, critical curves and deformation cross section match the exact solutions with a given accuracy. Although these quantities are useful for strong lensing applications, it is important to determine a domain of validity for arcs/finite sources. For example, Habara & Yamamoto (2011) investigated the domain of validity of the Perturbative Approach for extended circular sources. It is argued that Perturbative Approach can be used for sources with radius $\lesssim 0.2\, x_{\rm E}$ up to $\varepsilon \simeq 0.3$. This result should be extended for generic configurations probing the space of the source and lens parameters and their relative position. We expect that the limits here obtained can be connected to the domain of validity for arcs providing guidance to the exploration of this wider parameter space. The systematic application to arcs and connection to the current results is left for a subsequent work. It is also important to check whether the criterion established here for the $\mathcal{D}^2$ threshold can be applied to other lens models, so that we have an *a priori* criterium for the domain of validity of the Perturbative Approach regardless of the specific model.

The usefulness of the Perturbative Approach justifies the search for a determination its accuracy and limit of applicability. Once this is established we will be able to safely use this promising technique in a number of applications, within its domain of validity.

ACKNOWLEDGMENTS

HSDM is funded by the Brazilian agencies FAPERJ (E-26/101.784/2010), CNPq (PDJ/162989/2011-3), and the PCI/MCTI program at CBPF (301.860/2011-4). GBC is funded by CNPq and CAPES. BM is supported by FAPERJ. MM is partially supported by CNPq (grant 312876/2009-2) and FAPERJ (grant E-26/110.516/2012). MSSG acknowledges the hospitality of the Centro Brasileiro de Pesquisas Físicas (CBPF), where part of this work was performed, and the PCI/MCTI program (170.524/2006-0). We also thank the support of the Laboratório Interinstitucional de e-Astronomia (LIneA) operated jointly by CBPF, the Laboratório Nacional de Computação Científica (LNCC), and the Observatório Nacional (ON) and funded by the Ministry of Science, Technology and Innovation (MCTI). MM acknowledges C. Alard for useful discussions regarding the Perturbative Approach for arcs. We thank Marcos Lima for useful discussions.

REFERENCES

Abbott T. et al., 2005, preprint (astro-ph/0510346)
Alard C. 2007, MNRAS, 382, L58
Alard C. 2008, MNRAS, 388, 375
Alard C. 2009, A&A, 506, 609
Alard C. 2010, A&A, 513, A39
Annis J. et al., 2005, preprint (astro-ph/0510195)
Bartelmann M., Weiss A., 1994, A&A, 287, 1
Bartelmann M., Steinmetz M., Weiss A. 1995, A&A, 297, 1
Bartelmann M. 1996, A&A, 313, 697
Bartelmann M. et al., 1998, A&A, 330, 1
Bartelmann M. et al., 2003, A&A, 409, 449
Bayliss, M. B., 2012, ApJ, 744, 156
Belokurov V., Evans N. W., Hewett P. C., Moiseev A., McMahon R. G., Sanchez S. F., King L. J. 2009, MNRAS, 392, 104
Blandford R.D., Kochanek C.S., 1987, ApJ, 321, 658
Boldrin M., Giocoli C., Meneghetti M, Moscardini L., 2012, MNRAS, 427, 3134
Cabanac R. A. et al. 2007, A&A, 461, 813
Caminha G.B. et al., 2013, in preparation
Comerford J.M. et al., 2006, ApJ, 642, 39
Dobler G., Keeton C. R., 2006, MNRAS, 365, 1243
Dúmet-Montoya H. S., 2011, PhD Thesis, CBPF
Dúmet-Montoya H. S., Caminha G.B., Makler M., 2012, A&A, 544, 83
Estrada J. et al., 2007, ApJ, 660, 1176
Fedeli C. et al., 2006, A&A, 447, 419
Furlanetto C. et al., 2012, arXiv:1210.4136, MNRAS in press
Furlanetto C. et al., 2013, A&A, 549, A80
Gilbank D. G., Gladders M. D., Yee H. K. C., Hsieh B. C., 2011, AJ, 141, 94

Gladders M. D., Hoekstra H., Yee H. K. C., Hall P. B., Barrientos L. F., 2003, ApJ, 593, 48
Golse G., Kneib J.-P., 2002, A&A, 390, 821
Golse G., Kneib J.-P., Soucail G., 2002, A&A, 387, 788
Grossman S. A., Saha P., 1994, ApJ, 431, 74
Habara Y., Yamamoto, K., 2011, Int. J. Mod. Phys. D, 20, 371
Hamana T., Futamase T., 1997, MNRAS, 286, L7
Hattori M., Watanabe K., Yamashita K., 1997, A&A, 319, 764
Hennawi J. F. et al., 2008, AJ, 135, 664
Horesh A., Maoz D., Hilbert S., Bartelmann M., 2011, MNRAS, 418, 54
Horesh A., Maoz D., Ebeling H., Seidel G., Bartelmann M., 2012, MNRAS, 406, 1318
Jullo E. et al., 2007, New Journal of Physics, 9, 447
Jullo E. et al., 2010, Sci, 329, 924
Kassiola A., Kovner I., 1993, ApJ, 417, 450
Kausch W., Schindler S., Erben T., Wambsganss J., Schwope A., 2010, A&A, 513, A8
Keeton C.R., 2001a, preprint(astro-ph/0102340)
Keeton C.R., 2001b, ApJ, 562, 160
Kneib J.-P. et al., 1993, A&A, 273, 367
Kneib J.-P., 2001, preprint (astro-ph/0112123)
Kneib J.-P., Van Waerbeke L., Makler M., Leauthaud A., 2010, CFHT programs 10BF023, 10BC022, 10BB009
Kovner I., 1989, ApJ, 337, 621
Kubo J. M. et al., 2010, ApJ, 724, L137
Luppino G. A., Gioia I. M., Hammer F., Le Fèvre O., Annis J. A., 1999, A&AS, 136, 117
Meneghetti M. et al., 2001, MNRAS, 325, 435
Meneghetti M.,Bartelmann M., Moscardini L., 2003, MNRAS, 340, 105
Meneghetti M. et al., 2007, MNRAS, 381, 171
Meneghetti M. et al., 2008, A&A, 482, 403
Miralda-Escudé J., 1993a, ApJ, 403, 497
Miralda-Escudé J., 1993b, ApJ, 403, 509
Mollerach S., Roulet E., 2002, Gravitational Lensing and Microlensing. World Scientific Publishing Co. Pte. Ltd.
More A., Cabanac R., More S., Alard C., Limousin M., Kneib J.-P., Gavazzi R., Motta V., 2012, ApJ, 749, 38
Navarro J. F., Frenk C. S., White S. D. M., 1996, ApJ, 462, 563
Navarro J. F., Frenk C. S., White S. D. M., 1997, ApJ, 490, 493
Oguri M., Taruya A., Suto Y., 2001, ApJ, 559, 572
Oguri M., 2002, ApJ, 573, 51
Oguri M., Lee J., Suto Y., 2003, ApJ, 599, 7; erratum ibid 2004, 608, 1175
Oguri, M. 2010, PASJ, 62, 1017
Peirani S., Alard C., Pichon C., Gavazzi R., Aubert D., 2008, MNRAS, 390, 945
Petters A., O., Levine H., Wambsganss J., 2001, Singularity Theory and Gravitational Lensing. Birkhäuser, Boston
Rozo E. et al., 2008, ApJ, 687, 22
Schneider P., Elhers J., Falco E. E., 1992, Gravitational lenses. Springer-Verlag, Berlin
Sand, D. J., Treu, T., Ellis, R. S., Smith, G. P. 2005, ApJ, 627, 32
Smith, G. P., Kneib, J.-P., Smail, I., et al. 2005, MNRAS, 359, 417
Turner E. L., Ostriker J. P., Gott J. R., 1984, ApJ, 284, 1
van de Ven G., Mandelbaum R., Keeton C. R., 2009, MNRAS, 398, 607
Wayth R. B., Webster R. L., 2006, MNRAS, 372, 1187
Wen Z.-L., Han J.-L., Jiang Y.-Y., 2011, RAA, 11, 1185
Werner, M. C., An, J., Evans, N. W. 2008, MNRAS, 391, 668
Wiesner M. P., Lin H., Allam S. S. et al., 2012, ApJ, 761, 1
Wu X. P., Hammer F., 1993, MNRAS, 262, 187
Zaritsky D., Gonzalez A. H., 2003, ApJ, 584, 691